

Geophysical Research Letters



RESEARCH LETTER

10.1029/2018GL081316

Key Points:

- Removing the influence of atmospheric circulation variability reveals the thermodynamic component of observed precipitation trends
- The observed thermodynamic trend is in good agreement with anthropogenically forced trends from historical climate model simulations
- Our approach provides an alternative to formal “detection and attribution” methods for revealing anthropogenic changes in observations

Supporting Information:

- Supporting Information S1

Correspondence to:

C. Deser,
cdeser@ucar.edu

Citation:

Guo, R., Deser, C., Terray, L., & Lehner, F. (2019). Human influence on winter precipitation trends (1921–2015) over North America and Eurasia revealed by dynamical adjustment. *Geophysical Research Letters*, 46. <https://doi.org/10.1029/2018GL081316>

Received 13 NOV 2018

Accepted 24 FEB 2019

Accepted article online 4 MAR 2019

Human Influence on Winter Precipitation Trends (1921–2015) over North America and Eurasia Revealed by Dynamical Adjustment

Ruixia Guo^{1,2} , Clara Deser¹ , Laurent Terray³ , and Flavio Lehner¹

¹Climate and Global Dynamics Laboratory, National Center for Atmospheric Research, Boulder, CO, USA, ²Key Laboratory for Semi-arid Climate Change of the Ministry of Education, College of Atmospheric Sciences, Lanzhou University, Lanzhou, China, ³Climate, Environment, Coupling and Uncertainties group, Université de Toulouse, CERFACS/CNRS, Toulouse, France

Abstract Detecting and attributing a human influence on observed rainfall trends is a major challenge due to the presence of large amplitude internal variability on all time scales and by limited temporal and spatial data coverage. Here we apply a “dynamical adjustment” methodology to a gridded archive of monthly precipitation to estimate an anthropogenic influence on long-term (1920–2015) trends over North America and Eurasia during winter (November–March). This empirical approach aims to remove atmospheric circulation influences from precipitation variability and trends, thereby revealing the thermodynamically induced component as a residual. The geographical pattern and amplitude of this observed thermodynamic residual precipitation trend are in good agreement with anthropogenically forced trends obtained from ensembles of historical climate model simulations. Such consistency helps to reconcile observations and models and provides compelling evidence for a human influence on century-scale precipitation trends over North America and Eurasia during the cold season.

Plain Language Summary It is difficult to isolate the anthropogenic influence on long-term precipitation trends due to confounding effects from internal variability. Here we remove the influence of atmospheric circulation variability, which is primarily unforced, from observed precipitation trends using an empirical approach called “dynamical adjustment.” This removal isolates the thermodynamic component of observed precipitation trends as a residual. We find that this thermodynamic component is in good agreement with the anthropogenic component determined from historical simulations from climate models. Thus, we conclude that we are able to identify a human influence on observed century-scale precipitation trends over North America and Eurasia.

1. Introduction

Precipitation plays a crucial role in climate and sustains life on Earth. Without efforts to reduce greenhouse gas emissions from the burning of fossil fuels, humans will cause unprecedented changes in precipitation worldwide, with dire consequences for society, agriculture, and the environment (IPCC, 2013). Globally, precipitation is projected to increase at an approximate rate of 1–2% per K warming; regionally, however, rainfall changes will be more complex depending on local horizontal and vertical temperature gradients and associated changes in atmospheric circulation. For example, intensification and poleward expansion of the Hadley Circulation will lead to zonal-mean precipitation increases in the deep tropics and middle latitudes and reductions in the subtropics (Held & Soden, 2006; IPCC, 2013; O’Gorman & Schneider, 2009).

While theory and climate models provide a physical framework for understanding the projected changes in rainfall, detecting and attributing a human influence on observed rainfall trends is a major challenge (Hegerl et al., 2015; Knutson & Zeng, 2018; Sarojini et al., 2016). This challenge stems from the high degree of internal variability of precipitation at all time scales, and by limitations of the observational record including data quality issues and restricted spatial and temporal coverage (Hawkins & Sutton, 2009; Hegerl et al., 2015; Sarojini et al., 2016). Nonetheless, formal “detection and attribution” methods based on model “fingerprints” of externally forced signals have revealed a role for anthropogenic climate change in observed precipitation trends over limited latitudinal bands, regions, and seasons, including parts of the NH continents in winter and spring, as reviewed in Sarojini et al. (2016). Such methods have also been used to study changes

©2019. The Authors.

This is an open access article under the terms of the Creative Commons Attribution-NonCommercial-NoDerivs License, which permits use and distribution in any medium, provided the original work is properly cited, the use is non-commercial and no modifications or adaptations are made.

in the annual cycle of zonal-mean precipitation equatorward of 50° latitude during the satellite era (1979–2014), a period confounded by the global surface warming hiatus (Marvel et al., 2017). Most recently, Knutson and Zeng (2018) assessed the degree to which regional terrestrial precipitation trends are consistent with historical climate model simulations. They concluded that models possibly underestimate century-scale trends over extratropical land in comparison with observations, with important implications for the veracity of model projections over the coming decades. They ascribed the underestimation to a combination of model and forcing errors, in addition to data quality issues.

Here, we present a different approach to the problem of identification of a possible human influence on century-scale (1921–2015) precipitation trends over North America and Eurasia during the cold season using a “dynamical adjustment” methodology based on Constructed Circulation Analogs (CCAs). The benefit of this approach is that it provides an observationally based estimate of response to anthropogenic forcing that is independent of climate models. Versions of this methodology have been applied to terrestrial surface air temperatures to understand and attribute warming trends over the NH (Deser et al., 2016; Lehner et al., 2017; Smoliak et al., 2015) and to identify hotspots of land-atmosphere coupling (Merrifield et al., 2017). To the best of our knowledge, this is the first time dynamical adjustment has been used to study and attribute century-scale precipitation trends. O’Reilly et al. (2017) used dynamical adjustment to isolate residual thermodynamic effects of the Atlantic Multidecadal Oscillation upon European rainfall, while Lehner et al. (2018) used it to attribute changes in hydroclimate over the southwestern United States over the last few decades.

2. Data and Methods

2.1. Observational Data Sets

We use precipitation data from the Global Precipitation Climatology Centre (GPCC) version 7 (Schneider et al., 2015). This is a monthly gridded (2.5° latitude × 2.5° longitude) gauge-analysis product derived from quality-controlled station data covering the period 1901–2015. This data set includes information on the number of stations in each grid box for each month and year, which we use to mask out grid cells with insufficient data during our study period 1920–2015 using the criterion of at least one station with continuous data every decade on average from the 1920s through the 2000s. According to a recent comprehensive review of global precipitation data sets by Sun et al. (2018), GPCC contains approximately five times more station data than the Climate Research Unit archive (Harris et al., 2014; New et al., 2000), which is the only other century-long gridded gauge product. However, the patterns of precipitation trends based on Climate Research Unit are similar to those based on GPCC, with only small differences in amplitude, and our conclusions regarding dynamical and thermodynamic contributions to these trends are not affected by the choice of data set (see Figure S1).

For the dynamical adjustment procedure, we use monthly sea level pressure (SLP) data from the Twentieth Century Reanalysis (20CR) version 2c (Compo et al., 2011). This gridded product has a spatial resolution of 2° latitude × 2° longitude, and extends from 1920 to 2014. We have updated the 20CR through 2015 with data from ERA-interim (Dee et al., 2011). Long-term SLP trends over the NH extratropics in winter are considered more reliable in the 20CR than the ECMWF 20th Century Reanalysis (Poli et al., 2016) as documented by Bloomfield et al. (2018).

2.2. Model Data Sets

We make use of a 40-member ensemble of simulations with the Community Earth System Model, version 1 (CESM1), a fully coupled state-of-the-art climate model at a spatial resolution of approximately 1° in both latitude and longitude (Kay et al., 2015). Each ensemble member is subject to the same radiative forcing (historical for 1920–2005 and representative concentration pathway 8.5 emissions scenario for 2006–2100), but starts from slightly different atmospheric temperatures on 1 January 1920. Averaging across the 40 members provides a robust estimate of the model’s forced response to climate change (Deser et al., 2012). We also make use of the Fifth Coupled Model Intercomparison Project (CMIP5) archive (Taylor et al., 2012), which consists of 37 models with historical and representative concentration pathway 8.5 simulations. We select the first ensemble member from each of the 37 models and average them together to form the CMIP5 multi-model ensemble-mean, which we interpret as another estimate of the response to external radiative forcing.

2.3. Analysis Methods

Our study period is 1920–2015, dictated by the availability of the precipitation station data and the start year for the CESM1 ensemble. We compute monthly anomalies by subtracting the long-term (1920–2015) monthly means from the corresponding month of each year, and then form cold season (November through March) averages from the monthly anomalies. The 1921 cold season consists of data averaged from November 1920 through March 1921, and so on. We compute linear trends using least-squares regression analysis and assess statistical significance at the 90% confidence level using a two-tailed Student's t test. Similar results are obtained with more sophisticated trend fitting procedures such as Extended Empirical Model Decomposition (Wu & Huang, 2009; not shown). In addition, the results are not sensitive to the exact start date, with similar dynamically adjusted patterns for trends that begin in 1930, 1940, and 1950 (not shown). All model precipitation (SLP) data are regridded to the GPCC (20CR) grid using bilinear interpolation.

2.4. Dynamical Adjustment Technique

We remove the influence of atmospheric circulation variability from observed and simulated monthly precipitation following the CCA approach of Deser et al. (2016). First, we reconstruct the SLP pattern for a given month and year (T_i) using an optimal linear combination of SLP patterns in the same month from 40 randomly selected years in the data set (excluding the year in question) based on multiple linear regression. For example, to reconstruct the SLP pattern in January 1920, we optimally combine 40 randomly selected Januaries during 1921–2015. We then apply the same set of optimal linear weights to the corresponding precipitation fields to derive the “dynamically induced” component of precipitation at time T_i . This random selection and optimal reconstruction procedure is repeated 100 times (with replacement) for each month and year in order to sample different land and ocean states that might otherwise influence the estimate of dynamically induced precipitation. Finally, for each month and year, the 100 reconstructed SLP patterns and the accompanying dynamical-induced precipitation fields are averaged together, providing “best estimates” of these fields and to guard against overfitting.

The dynamical adjustment procedure is conducted separately for North America and Eurasia to improve the reconstruction of the SLP patterns and associated estimates of dynamically induced precipitation (see Figure S2 for the domains used). To obtain the thermodynamic contribution to precipitation in each month and year, we subtract the dynamically induced component from the total precipitation. It is important to note that the dynamically induced precipitation estimates include radiative and/or thermodynamic feedbacks that may arise from changes in, for example, cloud cover or land surface conditions that accompany the SLP patterns. Thus, the term dynamically induced precipitation refers to the combination of circulation influence and these potential local feedbacks (see Deser et al., 2016, and Lehner et al., 2017, for further discussion). We emphasize that no model information is used in our determination of the dynamical and thermodynamic contributions to observed precipitation.

We have examined the sensitivity of our results to the number of years chosen for our random samples, the number of repetitions used, and the size of the SLP domain and find only small differences for reasonable choices of these parameters, differences that are within the error of the method as determined by applying the same dynamical adjustment procedure to each ensemble member of CESM1 where the true forced response is known (see Figure S3).

3. Results

The map of observed winter precipitation trends during 1921–2015 is displayed in Figure 1. Northern Eurasia (north of approximately 40°N) shows widespread and statistically significant increases in winter precipitation during 1921–2015, with values exceeding 1.2–1.6 mm mo⁻¹ per decade west of the Ural Mountains and along the east coast, while southern Europe exhibits coherent albeit weaker amplitude drying trends that attain statistical significance over the eastern Mediterranean (Figure 1a). These precipitation trends occur in the context of changes in the large-scale atmospheric circulation, with negative SLP trends over northern Eurasia and positive SLP trends over the central North Atlantic extending into southwestern Europe (Figure 1a). Precipitation trends over North America are generally positive but statistically insignificant, accompanied by relatively weak trends in SLP (Figure 1a).

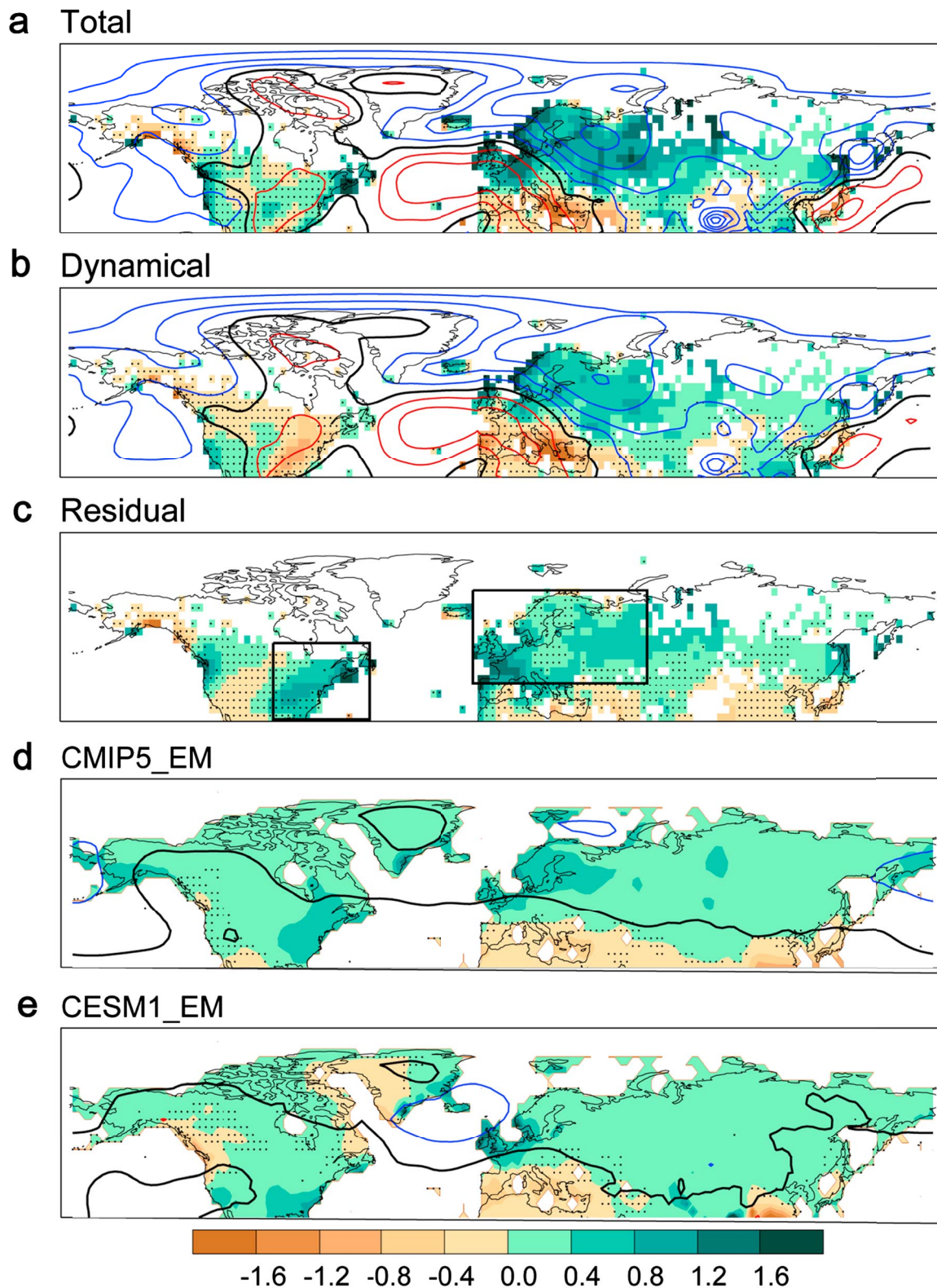


Figure 1. (a) Observed winter (November–March) precipitation (color shading; mm mo⁻¹ per decade) and SLP (contours, hPa per decade) trends during 1921–2015. (b) Dynamical contribution to (a). (c) Thermodynamic residual (a minus b). Ensemble-mean precipitation and SLP trends from (d) CMIP5 and (e) CESM1. In all panels, the SLP contour interval is 0.1 hPa per decade, with positive (negative) values in red (blue) and the zero contour in black. Stippled regions denote precipitation trends that are insignificant at the 90% confidence level based on a two-sided Student *t* test. The zero contour is suppressed for clarity on panel (c). CMIP5 = Fifth Coupled Model Intercomparison Project; CESM1 = Community Earth System Model, version 1; SLP = sea level pressure.

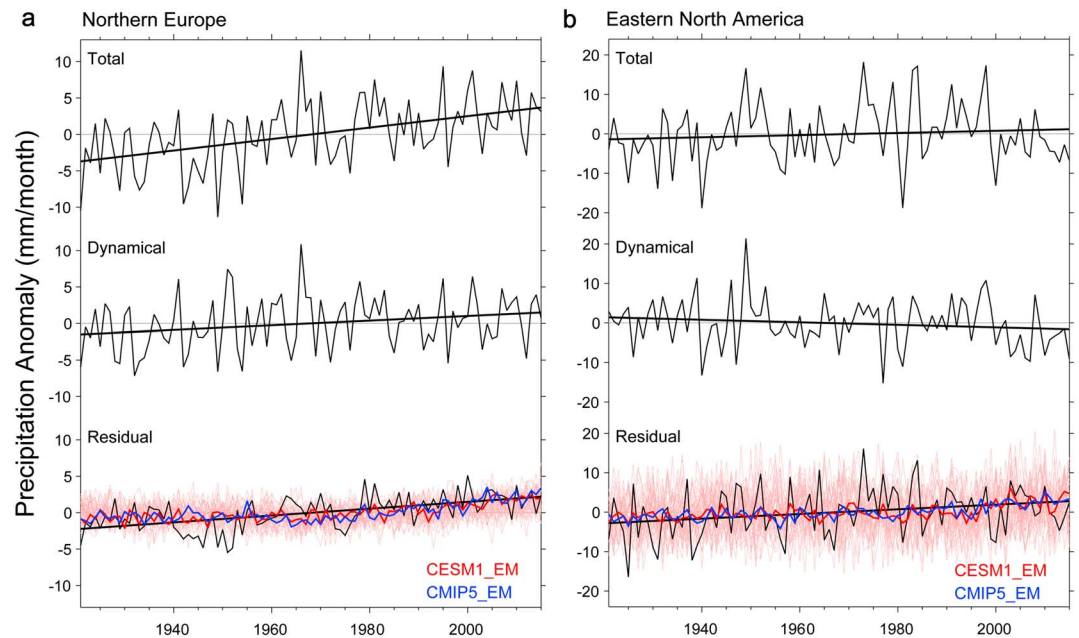


Figure 2. Observed time series of winter (November–March) precipitation anomalies (mm mo^{-1}) averaged over (a) Northern Europe and (b) Eastern North America (regions outlined in Figure 1c). The upper curve shows the total precipitation, middle curve shows the dynamical contribution, and the bottom curve shows the thermodynamic residual. Also shown are the best-fit linear trend lines. The thick red and blue curves show the CESM1 and CMIP5 ensemble-mean total precipitation time series, respectively, and the thin red curves show the thermodynamic residual time series for each of the 40 CESM1 ensemble members. CMIP5 = Fifth Coupled Model Intercomparison Project; CESM1 = Community Earth System Model, version 1.

The dynamical contribution to these observed trends as estimated with our CCA procedure is shown in Figure 1b. Atmospheric circulation changes account for approximately half of the wetting over northern Eurasia, and most of the drying over southern Europe (and extending northward into France and the southern United Kingdom), consistent with the cyclonic and anticyclonic SLP trends in these two regions, respectively (Figure 1b). These circulation-induced precipitation trends are generally statistically significant for magnitudes exceeding 0.4 mm mo^{-1} per decade (Figure 1b). Over North America, anticyclonic circulation trends produce significant drying in the east, while cyclonic trends contribute to wetting over the western United States (albeit insignificant; Figure 1b). It is evident by comparing the total (Figure 1a) and reconstructed (Figure 1b) SLP trends that our CCA procedure is highly skillful, with SLP trend differences near zero throughout the Northern Hemisphere (Figure 1c).

Subtracting the dynamically induced component of observed precipitation trends from the total yields an estimate of the thermodynamic contribution, hereafter referred to as “thermodynamic residual” (Figure 1c). The spatial pattern and amplitude of this observed thermodynamic residual precipitation trend are in good agreement with the radiatively forced component of trends simulated by climate models, here given by the ensemble-mean of 37 models in the CMIP5 (Figure 1d) and of the 40-member CESM1 (Figure 1e), more so than are the original (total) precipitation trends. For example, over Eurasia the thermodynamic residual trends show a more zonally uniform structure compared to the total trends, with precipitation increases (decreases) north (south) of approximately 35°N , similar to the models’ forced (ensemble-mean) patterns. In addition, the reduced magnitudes of the thermodynamic residual wetting and drying trends are in better agreement with the amplitudes of the models’ forced responses than are the total trends. Over North America, the thermodynamic residual trends show an area of significant positive values over the eastern third of the continent, a feature that is absent from the total trends and which corresponds well with the region of enhanced wetting in the models’ forced responses, especially CMIP5. The thermodynamic residual trends over the rest of North America are generally insignificant and do not resemble the models’ ensemble-mean trends. More quantitatively, the spatial correlation coefficient between the observed thermodynamic residual trend and the CMIP5 (CESM1) ensemble-mean trend is 0.63 (0.41), and the root-mean-square (rms) amplitude of

Table 1
Observed Total, Dynamical, and Thermodynamic Residual Precipitation (Top) Trends (1921–2015) and Associated 90% Confidence Intervals (mm mo^{-1} decade $^{-1}$) and (Bottom) Interannual Variance for Northern Europe and Eastern North America

Trend (1921–2015) (mm mo^{-1}) dec $^{-1}$	Observed total	Observed dynamical contribution	Observed thermodynamic residual	Ensemble-mean
				CMIP5
				CESM1
Northern Europe	0.79 ± 0.25	0.32 ± 0.22	0.47 ± 0.12	0.30 ± 0.06^a 0.29 ± 0.05^a
Eastern North America	0.27 ± 0.46	−0.32 ± 0.37	0.59 ± 0.36	0.44 ± 0.08^a 0.38 ± 0.10^a
Interannual variance (mm mo^{-1}) ²	Observed total	Observed dynamical contribution	Observed thermodynamic residual	Ensemble-mean thermo. resid.
				CMIP5
				CESM1
Northern Europe	20.2	13.1	5.2	3.0 ^b 2.4 ^b
Eastern North America	54.5	34.9	35.6	30.9 ^b 31.4 ^b

Note. For trend, values in bold font are significant at the 90% confidence level. For interannual variance, all data are detrended prior to computing the variance over the period 1921–2015. CMIP5 = Fifth Coupled Model Intercomparison Project; CESM1 = Community Earth System Model, version 1.

^aEnsemble-mean trend values and 90% confidence intervals based on (top) CMIP5 and (bottom) CESM1.

^bInterannual variance of thermodynamic residual precipitation averaged across all members of (top) CMIP5 and (bottom) CESM1.

the observed thermodynamic residual trend is 0.46 mm mo^{-1} per decade which is closer to the rms amplitude of the CMIP5 (0.31 mm mo^{-1} per decade) and CESM1 (0.33 mm mo^{-1} per decade) ensemble-mean trend than is the observed total trend (rms amplitude = 0.72 mm mo^{-1} per decade). Note that the ensemble-mean precipitation trends in CMIP5 and CESM1 show a high degree of statistical significance due to the large number of simulations averaged together, which reduces the noise from internal variability, while some noise remains in the observed thermodynamic residual due to errors in our dynamical adjustment methodology and potential internal thermodynamic influences.

The forced SLP trends in both CMIP5 and CESM1 are very weak compared to the observed SLP trends, underscoring that the radiatively forced precipitation trends in the two model ensembles are predominantly thermodynamic in origin (Figures 1d and 1e). This lends credence to our physical interpretation of the observed residual precipitation trends (Figure 1c). Indeed, we have verified that removing the forced SLP response (by subtracting the CESM1 or CMIP5 ensemble-mean SLP in each month and year) before performing dynamical adjustment on the observations does not appreciably alter the thermodynamic residual precipitation trends (see Figure S4).

To complement the trend maps, we show time series of total, dynamical, and thermodynamic residual cold season precipitation anomalies for two regions (outlined in Figure 1c): Northern Europe ($42\text{--}75^\circ\text{N}$, $12^\circ\text{W}\text{--}60^\circ\text{E}$) and Eastern North America ($30\text{--}55^\circ\text{N}$, $55\text{--}95^\circ\text{W}$). The significant upward trend in total precipitation over Northern Europe ($0.79 \pm 0.25 \text{ mm mo}^{-1}$ per decade) is superimposed upon large interannual variability (Figure 2a, top panel). Atmospheric circulation changes account for 40% of the total long-term trend, and 74% of the total interannual variance (Figure 2a, middle panel; Table 1), leaving a substantial upward trend ($0.47 \pm 0.12 \text{ mm mo}^{-1}$ per decade) and minimal variance in the residual time series (Figure 2a, bottom panel; Table 1). Note that the total interannual variance slightly exceeds the sum of the individual dynamical and thermodynamic residual interannual variances due to nonzero temporal correlation between these components (Table 1).

The magnitude of the observed thermodynamic residual trend for Northern Europe is similar to the anthropogenic (ensemble-mean) trends in CMIP5 and CESM1 (0.30 ± 0.06 and $0.29 \pm 0.05 \text{ mm mo}^{-1}$ per decade,

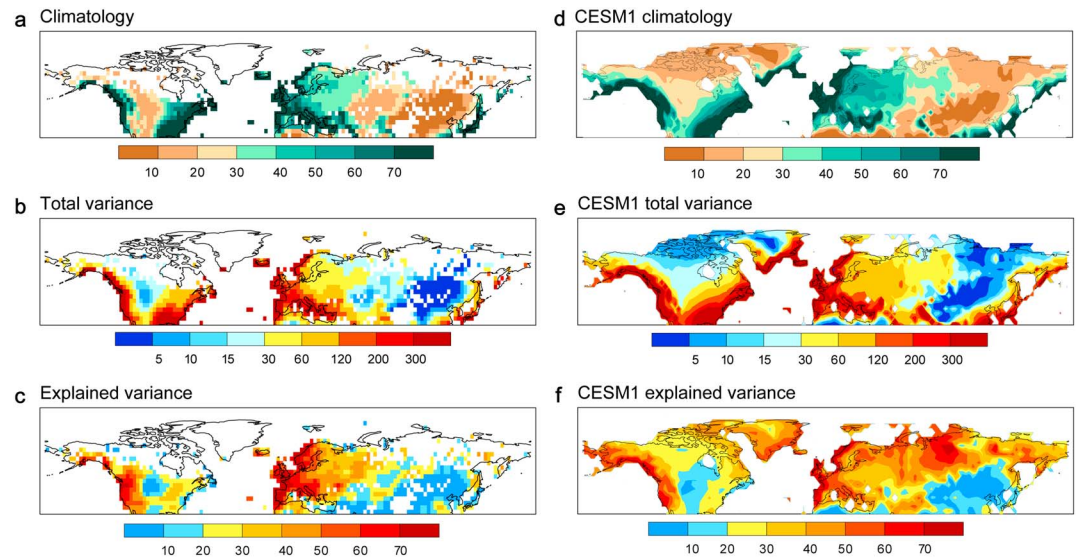


Figure 3. Observed and CESM1 winter (November–March) precipitation (a, d) climatology (mm mo^{-1}), (b, e) interannual variance (mm mo^{-1})², and (c, f) percentage of interannual variance explained by dynamical adjustment (%) based on detrended data during 1921–2015. Results for CESM1 are based on averaging across all 40 members of the ensemble. CMIP5 = Fifth Coupled Model Intercomparison Project; CESM1 = Community Earth System Model, version 1.

respectively; Table 1). In addition, the interannual variance of the observed (detrended) residual time series [$(5.2 \text{ mm mo}^{-1})^2$] is similar to that of the models' (detrended) residual time series [$(3.0 \text{ mm mo}^{-1})^2$ and $(2.4 \text{ mm mo}^{-1})^2$] for CMIP5 and CESM1, respectively, obtained by applying dynamical adjustment to each ensemble member and then averaging the residual variances across the members (Table 1). These results are visually apparent in Figure 2a (bottom panel), which shows that the observed residual time series lies within the spread of the 40 individual CESM1 residual time series in all but 7 years of the record (similar results are obtained for CMIP5; not shown). The CESM1 and CMIP5 ensemble-mean time series (thick red and blue curves in the bottom panel of Figure 2a) exhibit less interannual variability than the observed thermodynamic residual time series (Table 1), a reflection of the fact that with so many ensemble members, most of the noise from internal variability has been averaged out, while some noise remains in the observed thermodynamic residual due to errors in our dynamical adjustment methodology and potential internal thermodynamic influences.

Compared to Northern Europe, total precipitation over Eastern North America displays a much smaller (and statistically insignificant) upward trend ($0.27 \pm 0.46 \text{ mm mo}^{-1}$ per decade) and a higher level of interannual variance (Figure 2b, top panel; Table 1). Atmospheric dynamics causes a drying trend ($-0.32 \pm 0.37 \text{ mm mo}^{-1}$ per decade), leaving a statistically significant wetting trend in the residual time series ($0.59 \pm 0.36 \text{ mm mo}^{-1}$ per decade; Figure 2a, middle and bottom panels; Table 1). Like Northern Europe, the magnitude (and sign) of the residual trend is similar to the anthropogenic trends in CMIP5 and CESM1 (0.44 ± 0.08 and $0.38 \pm 0.10 \text{ mm mo}^{-1}$ per decade, respectively), and the residual variance is comparable to that in both model ensembles (Table 1). Indeed, the observed residual time series lies within the ensemble of residual time series from CESM1 (Figure 2b, bottom panel) and CMIP5 (not shown). A larger proportion of interannual variance remains in the observed residual time series for Eastern North America (65%) compared to Northern Europe (25%; Table 1).

Figures 3a and 3b show maps of observed cold season precipitation climatology and its interannual variance (based on detrended data), respectively. There is a strong correspondence between the climatology and the amplitude of variability. For example, coastal regions are wetter and more variable than continental interiors. The variance attributable to atmospheric dynamics maximizes over western North America and Eurasia, exceeding 50% within these areas and more than 70% along the European coast (Figure 3c). Less variance is explained elsewhere, even in the highly variable regions of eastern North America and Japan. Both CESM1 and CMIP5 show realistic simulations of the geographical patterns and amplitudes of precipitation climatology and total interannual variance, as well as the proportion of variance attributable to

dynamics (Figures 3d–3f and S5, respectively). The dominant modes of interannual precipitation variability over North America and Eurasia are associated with large-scale SLP anomaly patterns that are indicative of a circulation-driven influence (Figure S6); these relationships are realistically simulated by the models (Figure S7).

4. Summary and Discussion

To the best of our knowledge, this is the first use of dynamical adjustment to identify an anthropogenic influence on observed long-term (95-year) precipitation trends. In particular, we have applied a CCA-based procedure to estimate the dynamically induced portion of winter (November–March) precipitation trends during 1921–2015 over North America and Eurasia. Subtracting this dynamical component from the total trend yields the thermodynamic residual precipitation trend. The geographical pattern and amplitude of this observed thermodynamic residual trend are in good agreement with anthropogenically forced trends obtained from two different climate model large ensembles: the 37-model CMIP5 archive and the 40-member CESM1. In particular, the observed thermodynamic residual trends over Eurasia show a more zonally uniform structure compared to the total trends, with precipitation increases (decreases) north (south) of approximately 35°N, similar to the models' forced (ensemble-mean) patterns. In addition, the magnitudes of the residual wetting and drying trends are in better agreement with the models' forced responses than are the total trends. Over North America, the thermodynamic residual trends show enhanced wetting over the eastern third of the continent, similar to the forced responses in the model ensembles. In observations, this thermodynamic wetting trend is nearly completely offset by a dynamically induced drying trend.

The fact that the forced circulation (SLP) trends in both model ensembles are close to zero over the time period considered leads us to conclude that the dynamically induced portion of the observed precipitation trends is almost entirely internally generated. This, in turn, leads us to the interpretation that the observed residual precipitation trends are externally forced. The close similarity between the models' forced trends and the observed thermodynamic residual trend lends strong support to our inference and helps to reconcile models and observations. We emphasize that the dynamical adjustment procedure we have applied to observations is entirely independent of information from climate models, unlike other approaches such as those used in formal detection and attribution studies.

We have focused on winter in the extratropical NH for which internal circulation variability is large relative to the forced circulation response over the historical period. Our method may be less suited to future time periods, other seasons and regions for which radiatively forced circulation changes are more important (Seager et al., 2010; Byrne & O'Gorman, 2015; Simpson et al., 2016), although model information on forced circulation changes could be incorporated into the dynamical adjustment protocol. Finally, there is scope for improvement of our methodology by tailoring the SLP domain to different precipitation subregions and applying it to daily data.

Acknowledgments

We thank Isla Simpson and Angeline Pendergrass for useful discussions during the course of this work. The first author was supported by China Scholarship Council and National Natural Science Foundation of China (41722502, 41575006, 41521004, 91637312) and the China 111 project (B13045). NCAR is sponsored by the US National Science Foundation. Data supporting the conclusions can be obtained from the references, figures, the table, and the supporting information. We acknowledge the efforts of all those who contributed to producing the simulations and observational data sets. All CESM simulations are available online (earthsystemgrid.org). We thank the two anonymous reviewers for their helpful comments.

References

- Bloomfield, H. C., Shaffrey, L. C., Hodges, K. I., & Vidale, P. L. (2018). A critical assessment of the long-term changes in the wintertime surface Arctic Oscillation and Northern Hemisphere storminess in the ERA20C reanalysis. *Environmental Research Letters*, *13*, 094004. <https://doi.org/10.1088/1748-9326/aad5c5>
- Byrne, M. P., & O'Gorman, P. A. (2015). The response of precipitation minus evapotranspiration to climate warming: Why the “wet-get-wetter, dry-get-drier” scaling does not hold over land. *Journal of Climate*, *28*, 8078–8092. <https://doi.org/10.1175/JCLI-D-15-0369.1>
- Compo, G. P., Whitaker, J. S., Sardeshmukh, P. D., Matsui, N., Allan, R. J., Yin, X., et al. (2011). The twentieth century reanalysis project. *Quarterly Journal of the Royal Meteorological Society*, *137*, 1–28. <https://doi.org/10.1002/qj.776>
- Dee, D. P., Uppala, S. M., Simmons, A. J., Berrisford, P., Poli, P., Kobayashi, S., et al. (2011). The ERA-Interim reanalysis: Configuration and performance of the data assimilation system. *Quarterly Journal of the Royal Meteorological Society*, *137*, 553–597. <https://doi.org/10.1002/qj.828>
- Deser, C., Phillips, A., Bourdette, V., & Teng, H. Y. (2012). Uncertainty in climate change projections: The role of internal variability. *Climate Dynamics*, *38*, 527–546. <https://doi.org/10.1007/s00382-010-0977-x>
- Deser, C., Terray, L., & Phillips, A. S. (2016). Forced and internal components of winter air temperature trends over North America during the past 50 years: Mechanisms and implications. *Journal of Climate*, *29*, 2237–2258. <https://doi.org/10.1175/JCLI-D-15-0304.1>
- Harris, I., Jones, P. D., Osborn, T. J., & Lister, D. H. (2014). Updated high-resolution grids of monthly climatic observations – The CRU TS3.10 dataset. *International Journal of Climatology*, *34*, 623–642. <https://doi.org/10.1002/joc.3711>
- Hawkins, E., & Sutton, R. (2009). The potential to narrow uncertainty in regional climate predictions. *Bulletin of the American Meteorological Society*, *90*, 1095–1108. <https://doi.org/10.1175/2009BAMS2607.1>

- Hegerl, G. C., Black, E., Allan, R. P., Ingram, W. J., Polson, D., Trenberth, K. E., et al. (2015). Challenges in quantifying changes in the global water cycle. *Bulletin of the American Meteorological Society*, *96*, 1097–1115. <https://doi.org/10.1175/BAMS-D-13-00212.1>
- Held, I. M., & Soden, B. J. (2006). Robust responses of the hydrological cycle to global warming. *Journal of Climate*, *19*, 5686–5699. <https://doi.org/10.1175/JCLI3990.1>
- IPCC (2013). In T. F. Stocker, D. Qin, G.-K. Plattner, M. Tignor, S. K. Allen, J. Boschung, et al. (Eds.), *Climate Change 2013: The Physical Science Basis. Contribution of Working Group I to the Fifth Assessment Report of the Intergovernmental Panel on Climate Change* (1535 pp.). Cambridge, UK and New York: Cambridge University Press. <https://doi.org/10.1017/CBO9781107415324>
- Kay, J. E., Deser, C., Phillips, A., Mai, A., Hannay, C., Strand, G., et al. (2015). The community earth system model (CESM) large ensemble project: A community resource for studying climate change in the presence of internal climate variability. *Bulletin of the American Meteorological Society*, *96*, 1333–1349. <https://doi.org/10.1175/BAMS-D-13-00255.1>
- Knutson, T. R., & Zeng, F. R. (2018). Model assessment of observed precipitation trends over land regions: Detectable human influences and possible low bias in model trends. *Journal of Climate*, *31*, 4617–4637. <https://doi.org/10.1175/JCLI-D-17-0672.1>
- Lehner, F., Deser, C., Simpson, I. R., & Terray, L. (2018). Attributing the US Southwest's recent shift into drier conditions. *Geophysical Research Letters*, *45*, 6251–6261. <https://doi.org/10.1029/2018GL078312>
- Lehner, F., Deser, C., & Terray, L. (2017). Toward a new estimate of “time of emergence” of anthropogenic warming: Insights from dynamical adjustment and a large initial-condition model ensemble. *Journal of Climate*, *30*, 7739–7756. <https://doi.org/10.1175/JCLI-D-16-0792.1>
- Marvel, K., Biasutti, M., Bonfils, C., Taylor, K. E., Kushnir, Y., & Cook, B. I. (2017). Observed and projected changes to the precipitation annual cycle. *Journal of Climate*, *30*, 4983–4995. <https://doi.org/10.1175/JCLI-D-16-0572.1>
- Merrifield, A., Lehner, F., Xie, S. -P., & Deser, C. (2017). Removing circulation effects to assess central US land-atmosphere interactions in the CESM large ensemble. *Geophysical Research Letters*, *44*, 9938–9946. <https://doi.org/10.1002/2017GL074831>
- New, M., Hulme, M., & Jones, P. D. (2000). Representing twentieth century space-time climate variability. II: Development of 1901–1996 monthly grids of terrestrial surface climate. *Journal of Climate*, *13*, 2217–2238. [https://doi.org/10.1175/1520-0442\(2000\)013<2217:RTCSTC>2.0.CO;2](https://doi.org/10.1175/1520-0442(2000)013<2217:RTCSTC>2.0.CO;2)
- O’Gorman, P. A., & Schneider, T. (2009). The physical basis for increases in precipitation extremes in simulations of 21st-century climate change. *Proceedings of the National Academy of Sciences of the United States of America*, *106*, 14,773–14,777. <https://doi.org/10.1073/pnas.0907610106>
- O’Reilly, C. H., Woollings, T., & Zanna, L. (2017). The dynamical influence of the Atlantic multidecadal oscillation on continental climate. *Journal of Climate*, *30*, 7213–7230. <https://doi.org/10.1175/JCLI-D-16-0345.1>
- Poli, P., Hersbach, H., Dee, D. P., Berrisford, P., Simmons, A. J., Vitart, F., et al. (2016). ERA-20C: An atmospheric reanalysis of the twentieth century. *Journal of Climate*, *29*, 4083–4097. <https://doi.org/10.1175/JCLI-D-15-0556.1>
- Sarojini, B. B., Stott, P. A., & Black, E. C. L. (2016). Detection and attribution of human influence on regional precipitation. *Nature Climate Change*, *6*, 669–675. <https://doi.org/10.1038/nclimate2976>
- Schneider, U. et al., 2015: GPCP full data monthly product version 7.0 at 2.5°: Monthly land-surface precipitation from rain-gauges built on GTS-based and historic data.
- Seager, R., Naik, N., & Vecchi, G. A. (2010). Thermodynamic and dynamic mechanisms for large-scale changes in the hydrological cycle in response to global warming. *Journal of Climate*, *23*, 4651–4668. <https://doi.org/10.1175/2010JCLI3655.1>
- Simpson, I. R., Seager, R., Ting, M., & Shaw, T. A. (2016). Causes of change in Northern Hemisphere winter meridional winds and regional hydroclimate. *Nature Climate Change*, *6*, 65–70. <https://doi.org/10.1038/nclimate2783>
- Smoliak, B. V., Wallace, J. M., Lin, P., & Fu, Q. (2015). Dynamical adjustment of the Northern Hemisphere surface air temperature field: Methodology and application to observations. *Journal of Climate*, *28*, 1613–1629. <https://doi.org/10.1175/JCLI-D-14-00111.1>
- Sun, Q., Miao, C., Duan, Q., Ashouri, H., Sorooshian, S., & Hsu, K. L. (2018). A review of global precipitation data sets: Data sources, estimation, and intercomparisons. *Reviews of Geophysics*, *56*, 79–107. <https://doi.org/10.1002/2017RG000574>
- Taylor, K. E., Stouffer, R. J., & Meehl, G. A. (2012). An overview of CMIP5 and the experiment design. *Bulletin of the American Meteorological Society*, *93*, 485–498. <https://doi.org/10.1175/BAMS-D-11-00094.1>
- Wu, Z., & Huang, N. E. (2009). Ensemble empirical mode decomposition: A noise-assisted data analysis method. *Advances in Adaptive Data Analysis*, *01*, 1–41. <https://doi.org/10.1142/S1793536909000047>